Nanoscale Structure of the Oil-Water Interface

M. Fukuto,[1,*] B. M. Ocko,[1,†] D. J. Bonthuis,[2] R. R. Netz,[3] H.-G. Steinrück,[4]
D. Pontoni,[5] I. Kuzmenko,[6] J. Haddad,[7] and M. Deutsch[7]
[1]*Condensed Matter Physics and Materials Sciences Department and NSLS II, Brookhaven National Laboratory, Upton, New York 11973, USA*
[2]*Rudolf Peierls Centre for Theoretical Physics, Oxford University, 1 Keble Road, Oxford OX1 3NP, United Kingdom*
[3]*Department of Physics, Free University Berlin, D-14195 Berlin, Germany*
[4]*Stanford Synchrotron Radiation Lightsource, SLAC National Accelerator Laboratory, Menlo Park, California 94025, USA*
[5]*ESRF—The European Synchrotron, 71 Avenue des Martyrs, 38000 Grenoble, France*
[6]*Advanced Photon Source, Argonne National Laboratory, Lemont, Illinois 60439, USA*
[7]*Physics Department and Institute of Nanotechnology, Bar-Ilan University, Ramat-Gan 52900, Israel*
(Received 29 March 2016; revised manuscript received 20 September 2016; published 15 December 2016)

X-ray reflectivity (XR) and atomistic molecular dynamics (MD) simulations, carried out to determine the structure of the oil-water interface, provide new insight into the simplest liquid-liquid interface. For several oils (hexane, dodecane, and hexadecane) the XR shows very good agreement with a monotonic interface-normal electron density profile (EDP) broadened only by capillary waves. Similar agreement is also found for an EDP including a sub-Å thick electron depletion layer separating the oil and the water. The XR and MD derived depletions are much smaller than reported for the interface between solid-supported hydrophobic monolayers and water.

DOI: 10.1103/PhysRevLett.117.256102

Interfaces of hydrophobic with hydrophilic matter are ubiquitous in nature and in science. Understanding their structure is, therefore, of fundamental importance in biology, chemistry, materials science, and physics. The archetypical such interface, that of oil with water, attracted most attention [1–3]. Since oil and water do not mix, their laterally averaged, interface-normal electron density profile (EDP) has been considered to vary monotonically between those of the two bulks, over a width dictated by the capillary wave (CW) model [4]. This theory assigns the width to roughness created by thermally excited capillary waves, the amplitudes of which depend on the interfacial tension. However, XR [3,5,6] and neutron reflectivity studies [7] probing directly the EDP of interfaces of liquid alkanes with water dispute this simple model. For alkanes they yield broader interfaces than those predicted by CW theory. The excess broadening is attributed for the shorter alkanes to the molecule's gyration radius and for the longer *n*-alkanes to the bulk correlation length. Moreover, a long-standing theoretical prediction [8–12] of a low-density ("depletion") layer intruding at the oil-water interface and thus rendering its EDP nonmonotonic, eluded thus far conclusive experimental verification for *n*-alkanes. While the above-mentioned studies of liquid-liquid interfaces [3] found no evidence for such a layer, XR measurements [13–17] on the closely related interfaces of water with solid-supported hydrophobic SAMs support the existence of such a depletion layer. The exact nature, and origin, of this layer remains controversial, and is assigned either to water depletion [13–15] or to enrichment by the lower-density, hydrogen-rich terminal CH_3 groups of the monolayer [15,18]. Since both CH_3 and CH_2 groups are expected to be present at the *n*-alkane–water interface [2,19], the depletion behavior may differ compared to the SAMs [20]. To address these issues, we employed XR measurements and MD simulations to probe and model the interface of water with liquid normal alkanes [$CH_3(CH_2)_{n-2}CH_3$, denoted C_n, with $n = 6$, 12, and 16]. Our XR measurements, spanning a much-broader angular range than previous ones [6], support a monotonic EDP of a width coinciding with CW theory prediction, and place upper limits on both the depletion magnitude and the nonthermal (intrinsic) contribution to the interfacial width. In particular, the magnitude of the depletion, if it exists, is significantly less than that reported for the SAM-water systems. The simulations support a sub-Å depletion layer, and the simulated XR curve lies above the experimental one, especially at large wave vectors. This may originate from a subtle interplay between the effects of intrinsic roughness and the depletion layer on the XR.

XR measures $R(q_z)$, the reflected intensity fraction of an x-ray beam of wavelength λ incident on the interface at a grazing angle α, which yields the surface-normal scattering vector $q_z = (4\pi/\lambda)\sin\alpha$ [21]. For an ideally flat and abrupt liquid interface, broadened only by CWs [21–23],

$$R(q_z)/R_F(q_z) = \exp[-(\sigma q_z)^2], \tag{1}$$

where $R_F(q_z)$ is the Fresnel XR of an ideally flat and abrupt interface, and

$$\sigma^2 = \sigma_0^2 + \sigma_{\mathrm{CW}}^2 = \sigma_0^2 + k_B T/(2\pi\gamma)\ln(q_{\max}/q_{\min}), \tag{2}$$

where σ_{CW} is the CW-induced roughness, γ is the interfacial tension, σ_0 accounts for any nonthermal intrinsic interfacial roughness [22], and q_{min} and q_{max} are the CW lower and upper wave vector cutoffs [6,21]. In the experiments $q_{min} = q_z \Delta\beta/2$ is set by the spectrometer resolution [24], where $\Delta\beta$ is the angular acceptance of the detector and $q_{max} = \pi/r_0$ is approximated using the smallest molecular dimension ($r_0 = 2.5$ Å) [6]. For the simulations $q_{min} = 2\pi/L_{box}$ is set by the simulation box size, L_{box}.

A key enabling feature of the present measurements is the use of all-glass sample cells, composed of an inner cup (40–50 mm diam) residing concentrically within a taller outer cup (60–70 mm diam) and contained in a sealed, temperature controlled environment. The inner cup is first filled to its rim with ultrapure water. The outer cell is then filled with purified oils (passed through activated basic alumina columns) to a few mm above the water surface. Thus, the liquids contact only glass throughout the experiment. Well-established hot piranha glass cleaning procedures were employed [25]. No equivalent cleaning procedure is possible for the mylar, polycarbonate, and stainless steel materials used as cell components in the previous studies [5]. Further, it is well established that the x rays damage plastics through polymer bond breaking and oxidation, yielding soluble contaminants which may segregate to the liquid-liquid interface.

The XR measurements were carried out for C_{12} and C_{16} at ID15A (ESRF, France) and for C_6 at 9ID (APS, USA), respectively [24], at 25 ± 2 °C with beam heights of ~5 μm. The background was measured and subtracted using standard procedures [21] and involved rotating the detector horizontally from the specular position by an angle just greater than the resolution width in both in-plane directions, taking the average of the two values as the background.

In Fig. 1(a) we show the measured $R(q_z)/R_F(q_z)$ for C_{16}, C_{12}, and C_6 as open symbols where each data set shows a highly linear dependence of $\ln[R(q_z)/R_F(q_z)]$ on q_z^2. These results are in very good agreement with the CW model prediction of an ideally flat and abrupt interface, broadened by Gaussian roughness, but otherwise structureless. This calculation uses the instrumental resolution, q_{min} of 8.6×10^{-4}, 1.7×10^{-4}, and 8.4×10^{-5} Å^{-1}, for C_6, C_{12}, and C_{16}, respectively, evaluated at $q_z = 0.4$ Å^{-1} [24,26].

Moreover, Eq. (1) fits yield σ of 3.38 ± 0.30, 3.41 ± 0.15, and 3.54 ± 0.20 Å for C_6, C_{12}, and C_{16}, respectively, all close to their corresponding σ_{CW} values of 3.06, 3.31, and 3.41 Å. This good agreement suggests that $\sigma_0 \approx 0$ Å. Indeed, plots of Eq. (1) with fixed $\sigma = \sigma_{CW}$ [Fig. 1(a), solid lines] agree well with the measured data, over the full $0 \le q_z^2 \le 0.2$ Å^{-2} range measured, and without any adjustable parameters. However, for C_{12} a noticeable deviation from experiment is observed already for $\sigma_0 = \sqrt{2}\sigma_0^{air} = 1.56$ Å (short-dashed line), a value obtained as an upper limit by adding in quadrature the σ_0 of the water and of the alkane interfaces, assuming for both the same $\sigma_0^{air} = 1.1$ Å, measured for long-chain alkane-melt–air interfaces [22]. Thus, for a CW-broadened monotonic interfacial EDP, experiment clearly limits the nonthermal contribution to $\sigma_0 \lesssim 1.5$ Å. The discrepancy with the previous comprehensive XR study of C_n-water interfaces [6] is clear even for their smaller q range ($q_z^2 \le 0.07 - 0.12$ Å^{-2}). Their analysis yields σ_0 increasing with n, reaching 4.43 Å for $n = 16$ and they attribute the σ_0 to the molecules' radius of gyration.

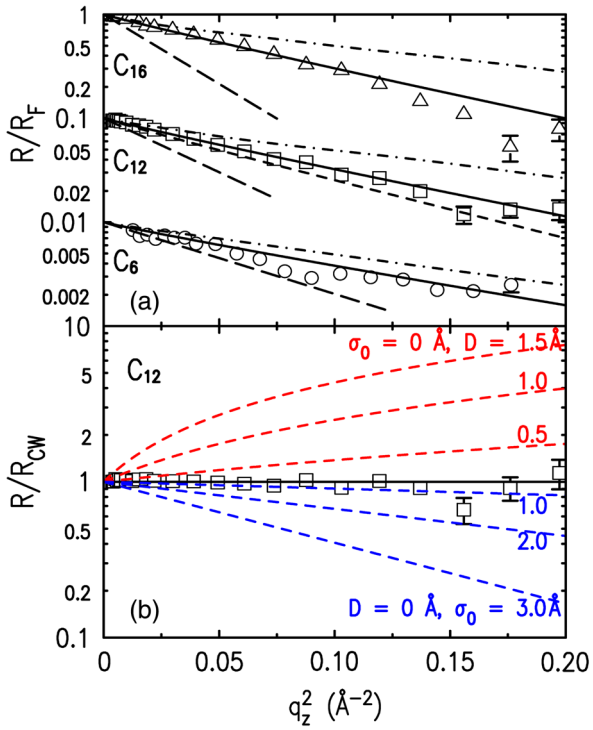

FIG. 1. (a) Fresnel-normalized reflectivity R/R_F for alkane (C_n)-water interfaces: measured (symbols), calculated (no-fit) CW theory prediction (R_{CW}/R_F), for $\sigma_0 = 0$ and $D = 0$ (solid lines), showing good agreement, and the same with $\sigma_0 = \sqrt{2}(1.1$ Å$) = 1.56$ Å (short-dashed line for C_{12}). The best fits of previous measurements [6] (long-dashed lines) show reduced q_z^2 range and systematic deviations from CW theory. MD simulations along with CW corrections are shown for $D^{MD} = 0.5$ Å (dot-dashed lines). (b) C_{12}-water R/R_{CW}: measured (symbols), and calculated (lines) for combinations of σ_0 and D. See text for discussion.

Whereas the analysis above is consistent with a CW-determined monotonic-EDP interface, it neglects the possibility of an interfacial electron depletion layer. For a thin layer of thickness D and density ρ_D, XR is insensitive to the specific values of D and ρ_D, and only sensitive to the z-integrated electron depletion, $\Gamma = D \times \Delta\rho$, where $\Delta\rho$ is the density difference between ρ_D and the average of water (ρ_w) and alkane (ρ_a) [17,18]. Including a depletion layer in the model and choosing a limiting $\rho_D = 0e/$Å^3 modifies Eq. (1) to

$$R_D/R_F = \exp[-(\sigma q_z)^2][1 + 4\varepsilon \sin^2(Dq_z/2)], \quad (3)$$

where $\varepsilon = \rho_w\rho_a/(\rho_w - \rho_a)^2$. At 25 °C, $\varepsilon = 6.9$, 15.6, and 19.2 for the water interface with C_6, C_{12}, and C_{16}, respectively. Accordingly, the impact of a depletion layer on the measured reflectivity is expected to increase with the chain length. R_D/R_F is well approximated by Eq. (1) with

$$\sigma^2 = \sigma_{\mathrm{CW}}^2 + \sigma_0^2 - \varepsilon D^2, \quad (4)$$

demonstrating that increasing σ_0 reduces R_D/R_F while increasing D increases R_D/R_F; see Fig 1(b). This mutual cancellation makes it difficult to distinguish EDPs having a thin ($D > 0$) and rough ($\sigma_0 > 0$) depletion layer from EDPs having a sharp ($\sigma_0 = 0$) water-oil interface and no depletion layer ($D = 0$), corresponding to the CW model with only a single, sharp interface at the oil-water interface.

Typical χ^2 maps for C_{12} [Fig. 2(a)], for a mesh of σ (or σ_0, with calculated σ_{CW}) and D [15,17,18], demonstrate the severe limits imposed by the data on the maximal D and σ_0. Statistical analysis [27,28] yields the best-fit $D^{\mathrm{bf}} = (0.46 \pm 0.46)$ Å and $\sigma_0^{\mathrm{bf}} = 1.9^{+1.3}_{-1.9}$ Å, and the 68% confidence level contour [Fig. 2(a)], corresponding to the conventional one-variable 1 standard deviation. Whereas D^{bf} is in good agreement with our simulations (see below), σ_0^{bf} much exceeds $\sigma_0^{\mathrm{air}} = 1.1$ Å found for the alkane-air interface [22]. We note that for $D = 0$ we obtain $0 < \sigma_0 = 0.9$ Å $< \sigma_0^{\mathrm{air}}$. Importantly, the $D^{\mathrm{bf}} = 0.46$ Å and the corresponding best-fit $\Gamma^{\mathrm{bf}} = 0.136e/\text{Å}^2$ are much lower than those of SAM-water interfaces [18,29]: 1.8 Å $\leq D \leq$ 3.8 Å and $0.30e/\text{Å}^2 \leq \Gamma \leq 0.67e/\text{Å}^2$.

Figure 2(b) shows several different model EDP profiles after including the effects of CW induced broadening. Note that the CW EDP with no depletion (red-dashed line) overlaps almost everywhere the EDPs with a depletion of $\Gamma = 0.136e/\text{Å}^2$ ($D = 0.46$ Å for $\rho_D = 0$) and $\sigma_0 = 1.9$ Å (black and blue-dashed lines). Thus, not only is the quality of the fits similar for EDPs with $D = 0$ and 0.46 Å as demonstrated by Figs. 2(a), but their EDPs are practically identical after inclusion of σ_0 for the latter case. We also note that the near-overlap between the two curves (blue and black) with the same value of Γ and different values of D provides further justification for Eq. (3).

Our MD simulations (GROMACS), done in the *NPT* ensemble at 300 K, employ SPC/E [30] and OPLS-AA [31] force fields for the water and C_n, respectively. We obtain bulk mass densities $m_i^{\mathrm{BULK}} = 645 \pm 1$, 741 ± 2, 764 ± 2, and 1000 ± 1 kg/m^3 for C_6, C_{12}, C_{16}, and H_2O, and oil-water interfacial tensions, calculated from the anisotropy of the pressure tensors, $\gamma_i = 51 \pm 2$, 54 ± 2, and 54 ± 2 mN/m, for C_6, C_{12}, and C_{16}. These values are within 1.5% (m_i^{BULK}) and 1% (γ_i) of their respective experimental values [6], demonstrating the simulations' quality. The simulation box size, L_{box} was either 40 (C_{12}) or 35 Å (C_6 and C_{16}).

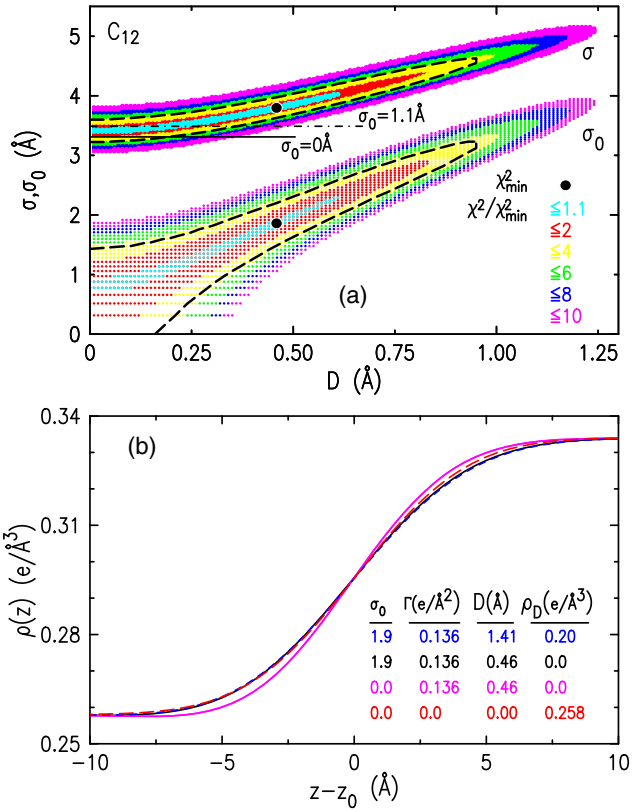

FIG. 2. (a) $\chi^2/\chi^2_{\mathrm{min}}$ maps for two-parameter models (σ, D) and (σ_0, D) for C_{12} that include a depletion layer, where the χ^2_{min} positions are shown by the black dots; σ for $\sigma_{\mathrm{CW}} = 3.31$ Å and $\sigma_0 = 0$, 1.1 Å (horizontal lines), and 68% confidence level contour (dashed lines). (b) C_{12}-water interface EDPs for (D, ρ_D) with various parameter combinations. The density profile is insensitive to the depth of the depletion for the same Γ (black and blue-dashed). The same depletion, with $\sigma_0 = 0$, provides a noticeably narrower profile (purple). The CW prediction with $\sigma_0 = 0$ (red-dashed) yields a profile similar to those for $\Gamma = 0.136e/\text{Å}^2$ and $\sigma_0 = 1.9$ Å. The value $0.258e/\text{Å}^3$ corresponds to the bulk C_{12} electron density.

The simulated mass density profiles $m(z)$ [Fig. 3(a)] were used to calculate the positions of the Gibbs dividing surfaces as $z_i^{\mathrm{GDS}} = z_j + \int_{z_j}^{z_i}[1 - m_i(z)/m_i^{\mathrm{BULK}}]dz$, where i, $j = w$ (water) or a (alkane), and $z_{i,j}$ are positions in the bulk of the respective liquids. From these, we obtain a depletion layer width as $D^{\mathrm{MD}} = z_a^{\mathrm{GDS}} - z_w^{\mathrm{GDS}} = 0.5 \pm 0.04$ Å for all C_n, yielding $\Gamma^{\mathrm{MD}} = 0.148e/\text{Å}^2$. These results are in good agreement with previous simulations using polarizable force fields [19], and with the experiment-derived D^{bf} and Γ^{bf} presented above.

The electron density profiles [Fig. 3(b)] are calculated as $\rho(z) = \sum_i \alpha_i n_i(z)$, where $n_i(z)$ and α_i are the number density and atomic number of atom i. For all C_n, $\rho(z)$ exhibits a dip at the interface, and clear oscillations on the alkane side with a C_n-independent period of ~4.5 Å. This period corresponds well to the bulk correlation lengths $\xi = 4.9$ (C_6), 4.5 (C_{12}), and 4.5 Å (C_{16}), calculated as

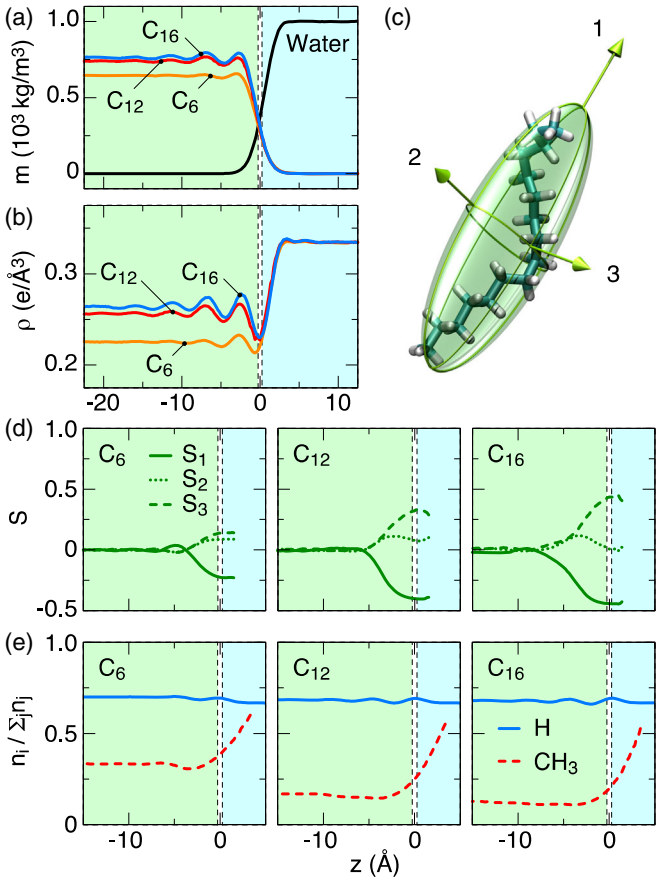

FIG. 3. (a) The mass density with the Gibbs dividing surfaces (black dashed lines). (b) The electron density $\rho(z)$. (c) A snapshot of a C_{16} molecule together with its three principal axes. (d) The order parameter S_k. (e) The relative densities of CH_3 and H.

$\xi = (l \times n_C^{\mathrm{BULK}})^{-\frac{1}{2}}$, where $l = 1.529$ Å is the C-C bond length and n_C^{BULK} is the C monomer bulk density [6].

The molecular orientation [Figs. 3(c)–3(d)] is calculated from the gyration tensor for each molecule, $G = \sum_{i,j}(\boldsymbol{r}_i - \boldsymbol{r}_j)(\boldsymbol{r}_i - \boldsymbol{r}_j)^T/(2N^2)$. i, j runs over all N atoms of the molecule, with $\boldsymbol{r}_i$ denoting atom i's position. Diagonalizing G is equivalent to fitting an ellipsoid to the molecule's shape. G's eigenvectors, labeled $k = 1, 2, 3$ for the largest, medium, and smallest eigenvalues, are the directions of the molecule's principal axes [Fig. 3(c)]. The order parameter is calculated as $S_k(z) = \langle 3\cos^2\theta_k - 1\rangle/2$, where θ_k is the angle between the kth eigenvector and the vector $(x, y, z) = (0, 0, 1)$, and $\langle \ldots \rangle$ indicates an average over all molecules at position z. $S_k = 1$ corresponds to an orientation perpendicular to the interface, whereas $S_k = -0.5$ corresponds to orientation parallel. Figure 3(d) shows that for all C_n the interface-adjacent molecules have their longest axis interface parallel, and their shortest axis mostly interface normal. The alignment is more pronounced for longer alkanes. The interface-adjacent density oscillations discussed above are likely caused by this strong interface-parallel molecular layering that also explains their periods' chain length independence. The short length scale of the oscillations resulting from the parallel orientation also explains that no molecular structure is visible in the XR profiles, and that the interfacial width is independent of the chain length, contrary to previous reports [6]. A chain-length-dependent σ would be expected for other alkane orientations.

Despite the interface-parallel molecular alignment, the relative CH_3 density at the interface is enhanced [Fig. 3(e)]. The relative density of species i is $n_i(z)/\Sigma_j n_j(z)$, with $n_{i,j}(z)$ being the number density of CH_3 groups or H atoms, and the sum running over all carbon groups (for CH_3), or over all atoms (for H). The CH_3 densities [dashed red lines in Fig. 3(e)] exhibit a roughly twofold increase in the interfacial region. This, in turn, increases the relative hydrogen content in the density-depleted interfacial layer [solid blue lines in Fig. 3(e)]. However, this effect is small, indicating that the $\rho(z = 0)$ dip in Fig. 3(b) is due to heavier-atom depletion rather than hydrogen enrichment.

The width, σ_{water}, of the simulated water electron density profiles is a measure of the CW roughness over the simulation's box size. Excellent fits (not shown) are obtained for C_6, C_{12}, and C_{16} with $\sigma_{\mathrm{water}} = 1.32 \pm 0.04$ Å, which is considerably smoother than the calculated CW value $\sigma_{\mathrm{CW}} = 1.8$ Å calculated using the molecular size of water, $r_0 = 2.5$ Å, and L_{box}. Agreement between the CW model and simulations is obtained with $r_0 = 10$ Å, suggesting that the shortest wavelength capillary mode may be influenced by the bending rigidity of the elongated alkane chains lying parallel to the interface.

To compare the simulated XR, $R_s(q_z)$, with experiment, we first correct the simulated $\rho(z)$ for the CW spectrum cutoff by the simulation box size. $\rho(z)$ is thus convoluted with a Gaussian of width σ_{CW} calculated from Eq. (2) with $q_{\max} = 2\pi/L_{\mathrm{box}}$. This accounts for the CW modes between $2\pi/L_{\mathrm{box}}$ and the resolution-determined $q_{\min}$, since these CW modes are not accounted for by the simulation. $R_s(q_z)$ is calculated from this corrected $\rho(z)$ using the Born approximation [21], $R_s(q_z)/R_F(q_z) = |(\rho_w - \rho_a)^{-1} \int [d\rho(z)/dz] \exp(-iq_z z) dz|^2$.

For all three chain lengths, using the simulated $\rho(z)$ with its depletion layer width of $D^{\mathrm{MD}} = 0.5$ Å, $R_s(q_z)/R_F(q_z)$ is higher [see dot-dashed lines in Fig. 1(a)] than both the measured reflectivity and the CW prediction. We note that excellent agreement of the simulations with the measured reflectivity can be obtained by either artificially reducing D found in the simulations, $D^{\mathrm{MD}} = 0.5$ Å to zero for all alkanes, or by incorporating *ad hoc* an additional non-thermal roughness σ_0, not exhibited by the simulations. For example, for C12, to reach a good simulation-experiment agreement in Fig. 1(a) requires increasing σ to 3.9 Å from the CW value of 3.3 Å. This, in turn, requires $\sigma_0 = \sqrt{(\sigma^2 - \sigma_{\mathrm{CW}}^2)} = 2.1$ Å, greater than the upper limit of $\sqrt{2}(1.1\ \text{Å}) = 1.56$ Å discussed above. There is no apparent justification for this increased broadening within the MD simulation since the capillary correction should

account for the smearing of the atomic positions, except for a small form factor contribution, which is neglible over the measured q_z range. Deviations from CW behavior have been detected by diffuse scattering [32] and reflectivity measurements on alcohol-water mixtures [33] at free liquid surfaces. These studies suggest that the CW model may need modifications for complex interfaces.

The major result of the present XR measurements is the mending of a long-standing apparent discrepancy of previous, shorter-range, XR measurements [6] with the CW theory. However, due to the shallow minimum in the χ^2, resulting from the mutually canceling effects of σ_0 and D, it is not possible to unambiguously distinguish between the CW-broadened monotonic interface model with a zero or small σ_0 and a model including a thin depletion layer with a larger σ_0. The simulations and experiments together suggest a gap in the range, $0 \leq D \leq 0.5$ Å, where the upper bound for D is 3–8 times smaller than those obtained for SAM-water interfaces [18,29]. Our results weaken the case for the existence of a significant depletion layer, thus illuminating the dichotomy between interfaces of water with solid-supported SAMs and with liquid alkanes. Although the simulations overestimate the measured R/R_F, they provide valuable information on the interface-adjacent orientation of the alkane molecules and on hydrogen enrichment at the interface. A better separation of the interfacial roughness into a thermal and nonthermal contribution, and a better understanding of the simulation-experiment discrepancy, would require extensive temperature-dependent XR measurements and simulations, preferably over a larger range of alkane length.

We thank V. Honkimaki and H. Reichert for discussions and advice, and gratefully acknowledge support by the U.S. Department of Energy, Office of Basic Energy Sciences, under Contracts No. DE-SC0012704 (M. F., B. M. O) in the CMPMS and NSLS II Departments at BNL and DE-AC02-06CH11357 for beamtime and support at 9ID at the APS at ANL, the U.S.-Israel Binational Science Foundation, Jerusalem (M. D.) and the ESRF for beamtime at ID15A and for PSCM support.

*fukuto@bnl.gov
†ocko@bnl.gov

[1] D. Chandler, Nature (London) **437**, 640 (2005).
[2] F. Bresme, E. Chacon, P. Tarazona, and K. Tay, Phys. Rev. Lett. **101**, 056102 (2008).
[3] K. Kashimoto, J. Yoon, B. Hou, C.-h. Chen, B. Lin, M. Aratono, T. Takiue, and M. L. Schlossman, Phys. Rev. Lett. **101**, 076102 (2008).
[4] F. P. Buff, R. A. Lovett, and F. H. Stillinger, Phys. Rev. Lett. **15**, 621 (1965).
[5] D. M. Mitrinovic, Z. Zhang, S. Williams, Z. Huang, and M. Schlossman, J. Phys. Chem. B **103**, 1779 (1999).
[6] D. M. Mitrinovic, A. M. Tikhonov, M. Li, Z. Q. Huang, and M. L. Schlossman, Phys. Rev. Lett. **85**, 582 (2000).
[7] A. Zarbakhsh, J. Bowers, and J. R. Webster, Langmuir **21**, 11596 (2005).
[8] F. H. Stillinger, J. Solution Chem. **2**, 141 (1973).
[9] K. Lum, D. Chandler, and J. D. Weeks, J. Phys. Chem. B **103**, 4570 (1999).
[10] P. Ball, Nature (London) **423**, 25 (2003).
[11] D. Chandler, Nature (London) **445**, 831 (2007).
[12] S. I. Mamatkulov, P. K. Khabibullaev, and R. R. Netz, Langmuir **20**, 4756 (2004).
[13] M. Mezger, H. Reichert, S. Schoder, J. Okasinski, H. Schroder, H. Dosch, D. Palms, J. Ralston, and V. Honkimaki, *Proc. Natl. Acad. Sci. U.S.A.* 103, 18401 (2006).
[14] A. Poynor, L. Hong, I. K. Robinson, S. Granick, Z. Zhang, and P. A. Fenter, Phys. Rev. Lett. **97**, 266101 (2006).
[15] M. Mezger, F. Sedlmeier, D. Horinek, H. Reichert, D. Pontoni, and H. Dosch, J. Am. Chem. Soc. **132**, 6735 (2010).
[16] S. Chattopadhyay, A. Uysal, B. Stripe, Y.-g. Ha, T. J. Marks, E. A. Karapetrova, and P. Dutta, Phys. Rev. Lett. **105**, 037803 (2010).
[17] A. Uysal, M. Chu, B. Stripe, A. Timalsina, S. Chattopadhyay, C. M. Schleputz, T. J. Marks, and P. Dutta, Phys. Rev. B **88**, 035431 (2013).
[18] B. M. Ocko, A. Dhinojwala, and J. Daillant, Phys. Rev. Lett. **101**, 039601 (2008).
[19] C. D. Wick, T.-M. Chang, J. A. Slocum, and O. T. Cummings, J. Phys. Chem. C **116**, 783 (2012).
[20] R. Godawat, S. N. Jamadagni, and S. Garde, *Proc. Natl. Acad. Sci. U.S.A.* 106, 15119 (2009).
[21] P. S. Pershan and M. L. Schlossman, *Liquid Surfaces and Interfaces: Synchrotron X-ray Methods* (Cambridge University Press, Cambridge, England, 2012). M. Deutsch and B. M. Ocko, *Encyclopedia of Applied Physics* (VCH, New York, 1998), Vol. 23.J. Als-Nielsen and D. McMorrow, *Elements of Modern X-ray Physics* (Wiley, New York, 2001).
[22] B. M. Ocko, X. Z. Wu, E. B. Sirota, S. K. Sinha, and M. Deutsch, Phys. Rev. Lett. **72**, 242 (1994).
[23] P. S. Pershan, J. Phys. Chem. B **113**, 3639 (2009).
[24] The energy (keV), sample to detector distance (mm), and vertical slits settings (mm), are (22.1, 920, 4), (69.75, 1200,1), and (69.75,1200, 0.5) for C_6, C_{12}, and C_{16}, respectively.
[25] W. Kern, *Handbook of Semiconductor Wafer Cleaning Technology* (Noyes Publications., Park Ridge, NJ, 1993).
[26] $q_{\min}$ was evaluated close to the highest q_z measured, where the effect of roughness on the reflectivity was the greatest.
[27] W. H. Press, S. A. Teukolsky, W. T. Vetterling, and B. P. Flannery, *Numerical Recipes in C: The Art of Scientific Computing*, 2nd ed. (Cambridge University Press, New York, NY, 1992).
[28] K. A. Brownlee, *Statistical Theory and Methodology*, 2nd ed. (Wiley, New York, NY, 1965).
[29] A. Poynor, L. Hong, I. K. Robinson, S. Granick, P. A. Fenter, and Z. Zhang, Phys. Rev. Lett. **101**, 039602 (2008).
[30] H. J. C. Berendsen, J. R. Grigera, and T. P. Straatsma, J. Phys. Chem. **91**, 6269 (1987).
[31] W. L. Jorgensen, D. S. Maxwell, and J. Tirado-Rives, J. Am. Chem. Soc. **118**, 11225 (1996).
[32] C. Fradin, A. Braslau, D. Luzet, D. Smilgies, M. Alba, N. Boudet, K. Mecke, and J. Daillant, Nature (London) **403**, 871 (2000).
[33] D. Vaknin, W. Bu, J. Sung, Y. Jeon, and D. Kim, J. Phys. Condens. Matter **21**, 115105 (2009).